Smart Mater. Struct. **19** (2010) 045003 (10pp) doi:10.1088/0964-1726/19/4/045003

Design and characterization of an electromagnetic energy harvester for vehicle suspensions

Lei Zuo, Brian Scully, Jurgen Shestani and Yu Zhou

Department of Mechanical Engineering, State University of New York at Stony Brook, Stony Brook, NY 11794, USA

E-mail: lei.zuo@stonybrook.edu

Received 6 October 2009, in final form 20 January 2010
Published 25 February 2010
Online at stacks.iop.org/SMS/19/045003

Abstract

During the everyday usage of an automobile, only 10–16% of the fuel energy is used to drive the car—to overcome the resistance from road friction and air drag. One important loss is the dissipation of vibration energy by shock absorbers in the vehicle suspension under the excitation of road irregularity and vehicle acceleration or deceleration. In this paper we design, characterize and test a retrofit regenerative shock absorber which can efficiently recover the vibration energy in a compact space. Rare-earth permanent magnets and high permeable magnetic loops are used to configure a four-phase linear generator with increased efficiency and reduced weight. The finite element method is used to analyze the magnetic field and guide the design optimization. A theoretical model is created to analytically characterize the waveforms and regenerated power of the harvester at various vibration amplitudes, frequencies, equilibrium positions and design parameters. It was found that the waveform and RMS voltage of the individual coils will depend on the equilibrium position but the total energy will not. Experimental studies of a 1:2 scale prototype are conducted and the results agree very well with the theoretical predictions. Such a regenerative shock absorber will be able to harvest 16–64 W power at 0.25–0.5 m s^{-1} RMS suspension velocity.

(Some figures in this article are in colour only in the electronic version)

1. Introduction

Among all the sources of pollutants in the atmosphere, automobiles have proved to contribute the most throughout the United States, for example, 70% of the carbon monoxide, 45% of the nitrogen oxide and 34% of the hydrocarbon pollution [1, 2]. Transportation accounts for 70% of the oil consumed in the United States (DOE data [3]), and 62% of this portion is used by automobiles [3, 4]. However, only 10–16% of the available fuel energy is used to drive the vehicle, i.e. to overcome the resistance from road friction and air drag (DOE and EPA data [5]).

Besides engine cycle efficiency, one important mechanism of energy loss in automobiles is the dissipation of kinetic energy during vehicle vibration and motion. In the past hundred years, the automotive industry has been working hard to dissipate the motion and vibration energy into *waste heat* by optimal design of braking and suspension systems, and by employing active controls like anti-lock braking systems or active suspensions. During the past ten years, energy recovery from braking has achieved great commercialization success in hybrid vehicles. However, regenerative vehicle suspensions, which have the advantage of continuous energy recovery, have not come into practice.

The shock absorber, an energy dissipating device, is used in parallel with the suspension spring to reduce the vibration excited by road irregularities or during acceleration and braking. The research about energy recovery from vehicle suspensions began more than ten years ago, first as an auxiliary power source for active suspension control, and later also as energy regenerating devices in their own accord. Suda *et al* [6, 7] investigated a self-powered active suspension control system, in which one motor is used to generate the energy and another motor is used to control the vibration in another

 © 2010 IOP Publishing Ltd Printed in the UK & the USA

stage. Nakano and Suda [8] later applied it to a truck cab suspension, in which they harvested the energy from the front suspension with an electric motor and a capacitor; this energy is then used to power another actuator for the cab suspension. Numerical simulation shows that the performance of this combined self-powered system is better than a passive or semi-active system. Nakano *et al* [9] also investigated the self-power vibration control using a single motor, in which a variable resistor, a charging capacitor and relay switches were used to control the motor force to follow the desired skyhook damping force. Jolly and Margolis [10, 11] classified subsystems as passive, regenerative and active, and potential performances and applications were discussed, including an energy regenerative control for a hydraulic seat suspension. Okada *et al* [12] proposed an active-regenerative control for suspension, in which energy is regenerated at high speed motion, and active control is used to provide damping at low speed when the regenerative voltage is smaller than the battery voltage. They realized that the vehicle vibration is mostly at low frequency and therefore the active control always consumes more energy than what is regenerated. To boost the regenerative voltage at low motion speed, Kim and Okada [13] introduced a PWM-modulated step-up chopper, which consisted of a small inductor and a high frequency switch. Graves *et al* [14] studied linear electromagnetic motor regenerative shock absorbers. They also noticed that the device output voltage must be large enough to overcome the barrier potential of the storage device. Goldner *et al* [15] did some preliminary studies on the energy recovery in vehicles by using a simple regenerative shock absorber composed of a single magnet and coils. They estimated the recoverable energy for a 2500 lb vehicle with an average speed of 20 m s^{-1} (45 mph) is about 20%–70% of the power that is needed for such a vehicle to travel on a typical highway at 45 mph. In addition to academia, the industry has also attempted to bring active suspensions into practice by making use of some of the vibration energy and reducing the power consumption. For example, one feature in Bose's active suspension [16] is its regenerative power amplifiers, which allow power to flow into the linear electromagnetic motor and also allow power to be returned from the motor.

Paz [17] conducted a study of different configurations of linear induction generators for vehicle suspension. The author presented a design method for one configuration of a magnet and conductor set-up, which was calculated to have a theoretical efficiency of 46%: however, a prototype was not fabricated. Finite element analysis on this design would suggest that the actual efficiency would be significantly less than predicted as a result of its ineffective use of high magnetically permeable materials for certain components. Goldner *et al*'s [18] patent for an electromagnetic linear generator and shock absorber design was able to recover energy at a significant efficiency: however, its weight of 70 kg (154 lbs) may not be appropriate for a passenger vehicle. Gupta *et al* [19] designed and fabricated two sets of regenerative shock absorbers and tested them in a small all-terrain vehicle (125 kg). Their experiment indicated that the rotary configuration regenerated power at a much higher efficiency (21%) than the linear configuration: however, its bulky design makes it incompatible with a passenger car. To further magnify the motion and increase efficiency, regenerative absorbers composed of ball screw and rotational electric motors have been developed by a number of researchers [20–24]. This ball screw mechanism can significantly magnify the vibration motion: however, large forces will transfer from the wheel to the vehicle and a degradation of ride comfort occurs at frequencies above 7–10 Hz, even with active control, as can be seen in [25, 23].

This paper aims at designing, characterizing and testing a retrofit regenerative shock absorber that can recover the vibration energy at high efficiency with relatively low weight, and without loss of ride comfort. This paper is organized as follows. In section 2, we outline our design concept, present finite element analysis and optimization, and describe the theoretical modeling. In section 3 we describe the test set-up and experimental results of the prototype, in comparison with the theoretical predictions. Conclusions are then given in section 4.

2. Concept, design and analysis

In this section we will first give an overview of the prototype design, and discuss the voltage and power estimation. The magnetic finite element method is then used for the design optimization to increase the power density, and finally a refined model of the energy harvesting is presented.

2.1. Overview of the electromagnetic shock absorber

The regenerative shock absorber is in the configuration of a linear generator, as shown in figure 1(a). The mechanism converts the kinetic energy of suspension vibration between the wheel and a sprung mass into useful electrical power. The shock absorber consists mainly of a magnet assembly and a coil assembly. The magnet assembly is made of ring-shaped permanent magnets and ring-shaped high magnetically permeable spacers stacked on a rod of high reluctance material. The magnets are arranged with like-poles of adjacent magnets facing each other to redirect the magnetic flux in the radial direction, as seen in figure 1(b). A concentric outer cylinder made of high magnetically permeable material is used to reduce the reluctance of magnetic loops, to further increase magnetic flux density in the coils. The coil assembly is made of copper coils wound on a delrin tube. The coils are connected to a rectifier set-up. As the copper coils move inside the magnetic field, a voltage will be generated. The weight of the full-scale regenerative shock absorber is estimated at 28 kg.

2.2. Design consideration

Based on the requirements of the design, the energy harvester is modeled as a linear induction generator that incorporates shock absorber functions. Simplified analysis will be used to guide the design first, and more comprehensive finite element analysis (FEA) and modeling will be given in sections 2.3 and 2.4.

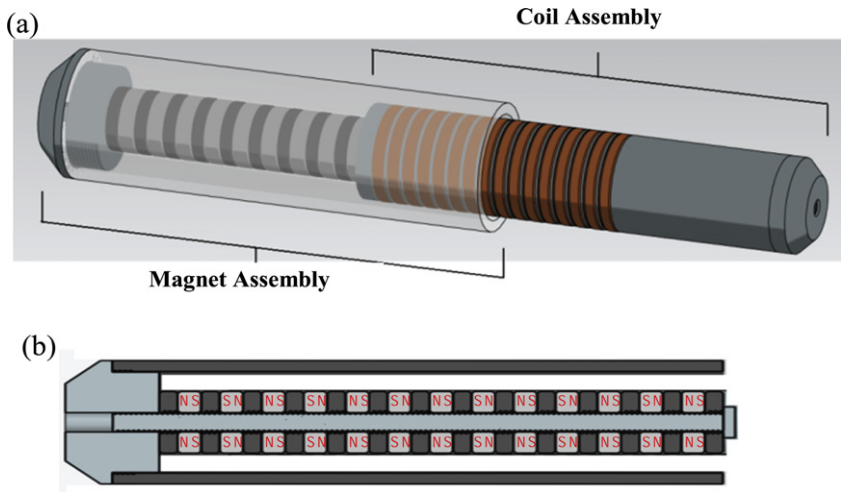

Figure 1. (a) Diagram of the linear electromagnetic shock absorber and (b) the cross section of the magnet assembly.

The EMF voltage V (V) generated by a conductor of length l (m) moving in a constant magnetic field B (T), at a constant velocity v (m s^{-1}), is given by

$$V = Bvl. \tag{1}$$

The maximum current, I (A), generated by the device with short circuit is given by the equation

$$I = \frac{V}{R} = \sigma B_{\mathrm{r}} v_z A_{\mathrm{w}} \tag{2}$$

where σ is the electrical conductivity (Ω m^{-1}) of the conductor, B_{r} is the magnetic field intensity in the radial direction, v_z is the constant relative velocity (m s^{-1}) of the coil conductor in the axial direction moving in the magnetic field and A_{w} is the cross-sectional area (m^2) of the conductor. The peak power, P, is calculated by combining equations (1) and (2):

$$P = VI = B_{\mathrm{r}}^2 v_z^2 \sigma l A_{\mathrm{w}}. \tag{3}$$

Equation (3) shows the importance of increasing the radial magnetic flux B_{r}. A double increase in B_{r} results in a quadratic increase in P. Therefore, the energy harvester is designed to have high magnetic flux by effectively using permanent magnets and high magnetically permeable materials in the magnet loop.

The magnet assembly consists of a magnet stack, spacers and concentric outer cylinder. The rare-earth permanent magnets (PM), specifically FeNdB grade N52, were chosen due to their high magnetic density (1.48 T) and availability. The PMs are stacked on a 7075 aluminum rod. Aluminum material was chosen because of its high reluctance property ($\mu = 1.27 \times 10^{-6}$ H m^{-1}) and its high tensile strength. The PMs are aligned with like-poles facing to produce a radially emitted magnetic flux. To reduce the effects of air in decreasing the radial flux in the coil conductor, high magnetically permeable 1018 steel spacers ($\mu = 875 \times 10^{-6}$ H m^{-1}) are inserted between each PM. Given the maximum allowable space of the shock absorber in typical vehicles, the PMs and steel spacers for this 1:2 prototype were selected to have an OD of 25.4 mm and ID 7.94 mm. Based on available sizes, the thickness of the PM is 6.35 mm. If we ignore the magnetic flux going through the high reluctance aluminum rod, the total radial flux emitted from the side of the spacer will equal the flux emitted from the PM pole surface:

$$\phi = 2B_{\mathrm{mag}} A_{\mathrm{pole}} = B_{\mathrm{spacer}} A_{\mathrm{side}} \tag{4}$$

where $A_{\mathrm{pole}} = \frac{\pi}{4}(D_{\mathrm{out}}^2 - D_{\mathrm{in}}^2)$ and $A_{\mathrm{side}} = \pi D_{\mathrm{out}} h_{\mathrm{spacer}}$.

The thickness of the spacer, h_{spacer}, was taken as 5.0 mm. The numbers of PMs, 12, and spacers, 13, were determined by the maximum compression limitations of the shock absorber based on sampling of mid-sized passenger cars. The outer cylinder was designed to increase the magnetic flux through the coils. The use of high magnetically permeable material will effectively 'pull' the flux away from the magnet stack and further increase radial flux density, as we will see in section 2.3. A 1018 low carbon steel tube was chosen for this purpose.

The coil assembly consists of a support tube and multiple coil windings. The tube moves relative to the magnet field due to vibrations in the vehicle suspension and generates a voltage. The support tube is made of delrin with high electrical resistance, instead of conventional metal. The reason is to eliminate eddy current energy loss in the support tube. The coils were designed to align with the magnet stack. The height of one coil is equal to half of the total height of a PM and a spacer. The total number of coils was determined to be 16, based on the maximum stroke of the shock absorbers of typical mid-size passenger cars. In this way 8 of the 12 magnets will be in the coil assembly range, and the half- and full-scale regenerative shock absorbers can maintain a constant performance of power generation for travels of 2 and 4 inches, respectively. The coil thickness, 5.85 mm, was determined from the space restriction of the typical shock absorber diameter. A copper coil of 250–300 turns and gauge of 30 AWG was used and the length l is

$$l = \pi D_{\mathrm{c}} N \tag{5}$$

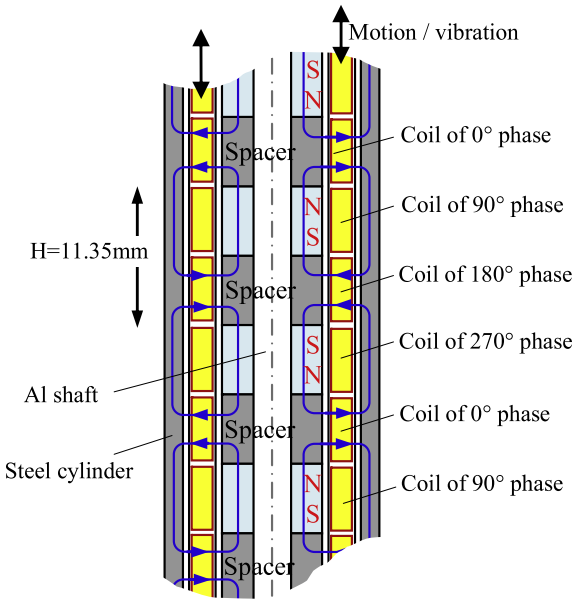

Figure 2. Diagram of the four-phase generator configuration: the coils move in the magnetic field during the vibration of vehicle suspensions.

where D_c is the average diameter of the coils and N is the number of turns which is determined as

$$N = \frac{\pi}{2\sqrt{3}}\frac{A_c}{A_w} = \frac{\pi}{2\sqrt{3}}\frac{4A_c}{\pi d^2} = \frac{2A_c}{\sqrt{3}d^2} \tag{6}$$

where d is the diameter of the wire, and A_c and A_w are the cross-sectional areas of the coil and wire, respectively. Thus, the peak voltage of one coil will be

$$V = \frac{2\pi B_r v_z D_c A_c}{\sqrt{3}d^2} \tag{7}$$

and the peak power will be

$$P = \frac{\pi^2 \sigma B_r^2 v_z^2 D_c A_c}{2\sqrt{3}}. \tag{8}$$

The peak output voltage is inversely proportional to the square of the wire diameter and the peak power will only depend on the total volume of conducting material in the coils.

All the coils together will form a four-phase design, as shown in figure 2. The 0° and 180° phases will generate maximum positive and negative voltages at the indicated position, and the 90° and 270° phases will have zero voltage. Though the voltage or power of each phase depends on the relative position of the coil assembly in the magnetic field, the total power generation, however, does not, which we will see in Experiment 4 of section 3.

2.3. Finite element analysis

Finite element analysis was conducted using the 2D FEA program *finite element method magnetics* [26] to calculate the magnetic flux intensity through the coils and to optimize the parameters obtained from the simplified analytical calculations. The effect of various materials with different magnetic permeabilities were modeled and analyzed. Figure 3 shows three diagrams of the theoretical flux intensity obtained using a 2D axisymmetric model of the initial and improved designs for the 1:2 scale prototype. The original design used a steel rod ($\mu = 875 \times 10^{-6}$ H m^{-1}) in the center of the magnet stack. However, through FEA it was found that its high permeability yielded the large flux intensity inside the rod, not in the copper coils. Thus, the rod material was changed to aluminum because of its much lower magnetic permeability ($\mu = 1.27 \times 10^{-6}$ H m^{-1}). This increases the flux intensity through the middle of the coils (3.87 mm to the outer surface of the magnets) from 0.196 to 0.231 T, or by 18%. Observing a certain amount of flux returns to the magnets before penetrating the coils, we add a high magnetically permeable outer cylinder made of soft steel. Figure 3(c) shows the magnetic flux of the FEA result. We see that the steel effectively contains the flux within the device and increases the flux intensity through the coils. With the high permeable outer cylinder, the radial flux intensities through the coils were further increased to 0.287 T, or by 24%. The flux intensities can be seen in figure 4. Therefore, the improved design results in a 46.4% increase of magnetic field intensity, which means 114% increase of the power density of the energy harvester. It should be noted that the steel outer cylinder is fixed together with the magnets instead of the coils, otherwise eddy current loss will occur inside the outer cylinder.

2.4. Refined modeling of regenerated voltage

The regenerated voltage on one coil of the shock absorber is

$$V = \int B_r v_z \, dl = v_z \int B_r \, dl = v_z(t) B_{ave}(z) L \tag{9}$$

where $B_{ave}(z, t)$ is the average of magnet field intensity B_r in the coil segment centered at position $z(t)$. Under harmonic vibration $v_z(t) = v_{max} \sin wt$, the coil position $z(t)$ will be shifted from the equilibrium position z_0:

$$z(t) = z_0 - (v_{max}/\omega) \cos \omega t. \tag{10}$$

Figure 4 shows the magnet field intensity B_r of the coil in the radial direction along the axial direction z. By taking the average in the segment of a coil (4.7 mm) in the magnetic field, we obtain the curve as shown in figure 5, which can be closely approximated by a cosine function:

$$B = B_0 \cos(\pi z / H) \tag{11}$$

where $B_0 = 0.25$ T and H is the sum of the thicknesses of a magnet and a spacer, 11.35 mm.

Plugging equations (10) and (11) into equation (9), we find the *instantaneous voltage* of one coil centered at equilibrium position z_0 in the regenerative shock absorber will be

$$V = B_0 L \cos\{\pi [z_0 - (v_{max}/\omega) \cos \omega t]/H\} v_{max} \sin \omega t. \tag{12}$$

Equation (12) characterizes the open circuit voltage of the individual coil of the proposed energy harvester as a function

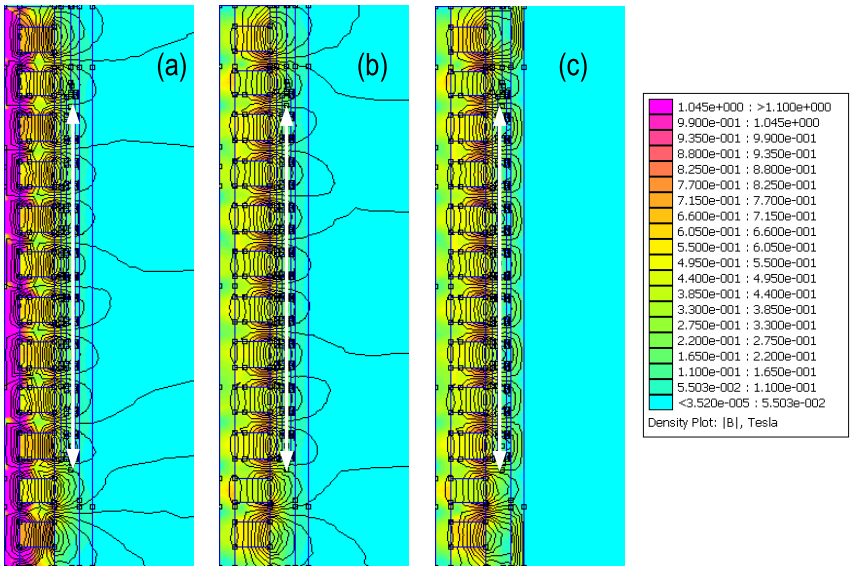

Figure 3. The magnetic flux intensity of the original and improved designs calculated with the finite element method, where the arrow shows the coils' position inside the magnetic field. (a) Steel center rod and no outer cylinder, (b) aluminum center rod and no outer cylinder, (c) aluminum center rod and steel outer cylinder.

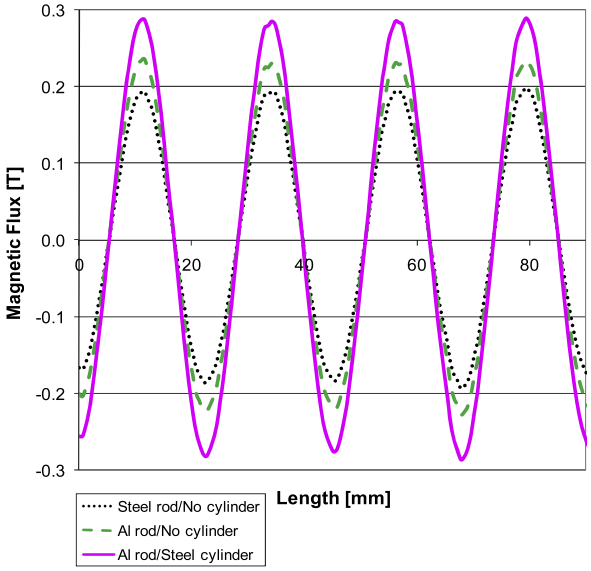

Figure 4. Magnetic flux through the middle of the coils in the radial direction obtained by using finite element analysis. The energy density of the harvester in the improved design will be more than doubled.

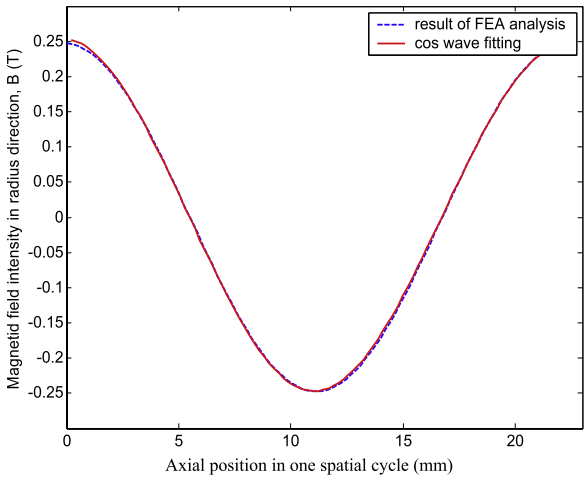

Figure 5. The magnet field intensity averaged over one coil direction in one space cycle $2H$ along the axial direction.

of time, position, magnetic intensity, geometrical parameters, and the suspension velocity and frequency. Some important characteristics will be observed and highlighted in section 3. This equation can be used to accurately estimate the harvested voltage, power and waveforms, as seen in section 3.

3. Analysis and experiments

3.1. Experiment set-up and mathematical modeling

The 1:2 scale regenerative shock absorber was fabricated based on the parameters derived from section 2. A test set-up was designed to characterize the voltage output and power output of the generator at various road conditions, as shown in figure 6. The magnet assembly of the shock absorber was mounted in the mover of a vibration shaker. The coil assembly was mounted to the top plate, which is fixed on the base of the vibration shaker. The position of the coil assembly can be adjusted via a $1/4''$-20 threaded rod. The shaker drives the relative motion between the magnet and coil assemblies via a $5\times$ power amplifier. Road conditions were simulated with a wavefunction generator. Waves at different frequencies and amplitudes were sent through the power amplifier to the vibration shaker. An oscilloscope was used to measure the output voltage, both peak and RMS values, of the shock absorber. The oscilloscope was also used to view the output waveforms generated from the shock absorber. A multimeter was used to measure current output.

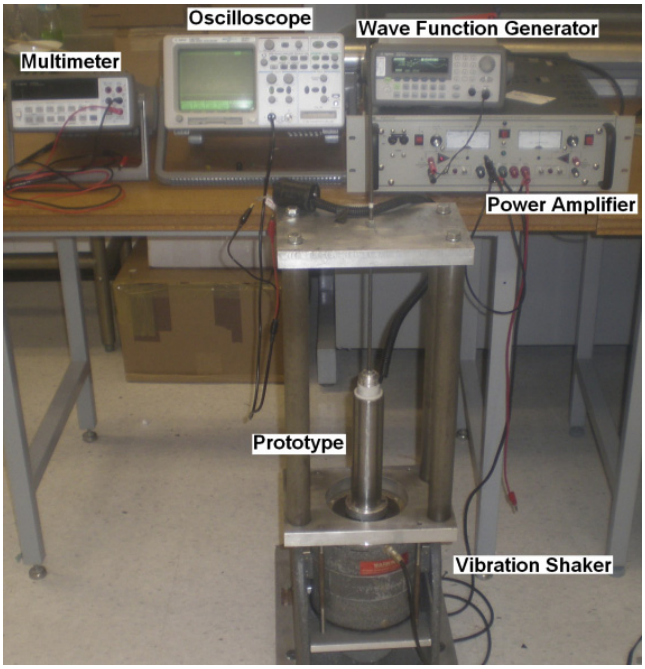

Figure 6. Experiment set-up with prototype.

A series of experiments were carried out to see the wave shapes, regenerated voltages and powers of the generated voltage at different vibration amplitudes, frequencies and equilibrium positions. To explain the results, we also created a mathematical model and made predictions using Matlab.

The shaker can be modeled as a single-DOF vibration system, as seen in figure 7. The vibration velocity v will depend on the frequency ω and driving voltage. If the inductance of the shaker is negligible, the regenerated voltage (open circuit) under shaker excitation $e_{\text{in}}(t) = e_{\text{in}} \sin \omega t$ will be

$$v = v_{\max} \sin \omega t, \text{ where}$$
$$v_{\max} = k_e \frac{\mathrm{j}\omega}{\omega_{\text{n}}^2 - \omega^2 + 2\mathrm{j}\zeta\omega_{\text{n}}\omega} e_{\text{in}} \tag{13}$$

where k_e is a constant. The natural frequency ω_{n} of the shaker is observed to be 13.5 Hz, while the damping ζ is contributed by the shaker's viscoelastic flexure guides, shaker's coil resister and the shock absorber's damping. We observe that the shaker is well damped inherently by the first two factors before we mount the shock absorber.

3.2. Experiment results

Experiment: waveform of the regenerated voltage. Let us look at equations (12) again. It indicates that the waveforms of the regenerated voltage of one coil do not necessarily have the same frequency as the excitation frequency ω. Instead, both the frequency and wave shapes will depend on the amplitude of vibration velocity $v_{\max}$, the equilibrium position z_0, the frequency ω and the thickness H of the magnet and the spacer. Figure 8 shows the waveforms of the regenerated voltage at different vibration amplitudes of 0° and 90° phases predicted by equation (12).

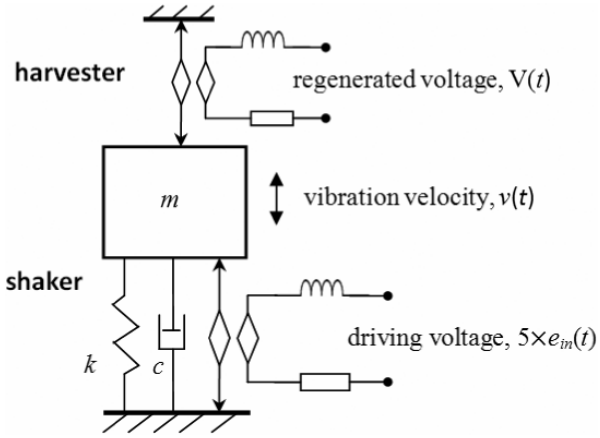

Figure 7. Model of the experiment set-up.

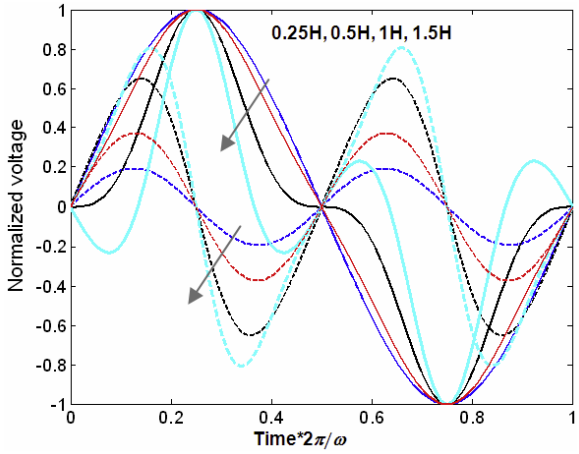

Figure 8. The normalized waveforms of regenerated voltage of one coil at 0° and 90° phases under peak-to-peak vibration amplitudes $2v_{\max}/\omega = 0.25H, 0.5H, 1H, 1.5H$, where $H = 11.35$ mm.

For the 0° phase coil which has the maximum magnetic intensity, $V = B_0 L \cos\{\frac{\pi v_{\max}}{H\omega} \cos \omega t\} v_{\max} \sin \omega t$. If the vibration amplitude is small $v_{\max}/\omega \ll H/\pi$ (at small shaker voltage input or high frequency), the regenerative voltage will approximate a sine wave $V = B_0 L |\frac{\mathrm{j}\omega}{\omega_{\text{n}}^2 - \omega^2 + 2\mathrm{j}\zeta\omega_{\text{n}}\omega} e_{\text{in}}| \sin \omega t$, and a 90° phase coil will have a double frequency wave:

$$V = B_0 L \cos\left\{\frac{\pi}{2} - \pi\left(\frac{v_{\max}}{\omega}\right) \cos \omega t / H\right\} v_{\max} \sin \omega t$$
$$= B_0 L \sin\left\{\left(\frac{\pi}{H}\right)\left(\frac{v_{\max}}{\omega}\right) \cos \omega t\right\} v_{\max} \sin \omega t$$
$$\approx B_0 L \frac{\pi V_{\max}^2}{2H\omega} \sin 2\omega t.$$

Such a prediction is confirmed by the experimental results, as seen in figure 9.

Equation (12) also indicates that, if the coils are not exactly in the 0°/180° or 90°/270° position, regenerated voltage under sinusoidal excitation will not be in a sinusoidal waveform, even if the vibration amplitude is very small. Figure 10 shows the wave shape of such phases.

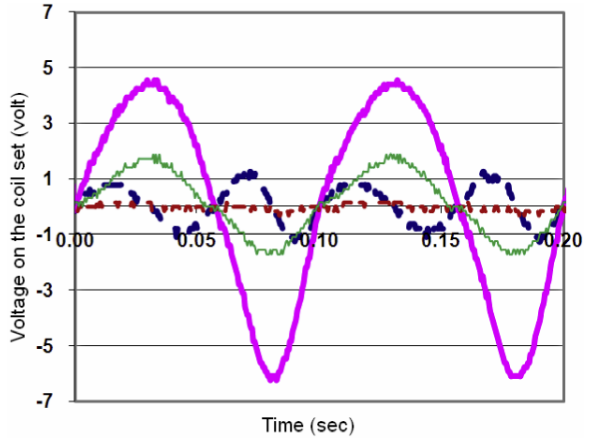

Figure 9. The recorded waveforms of regenerated voltages under 10 Hz excitation: 0° phase with $0.36H$ amplitude/0.6 V excitation (thicker solid), 90° phase with $0.36H$ amplitude (thicker dashed), 0° phase with $0.1H$ amplitude/0.2 V excitation (solid) and 90° phase with $0.1H$ amplitude (dashed). $H = 11.35$ mm.

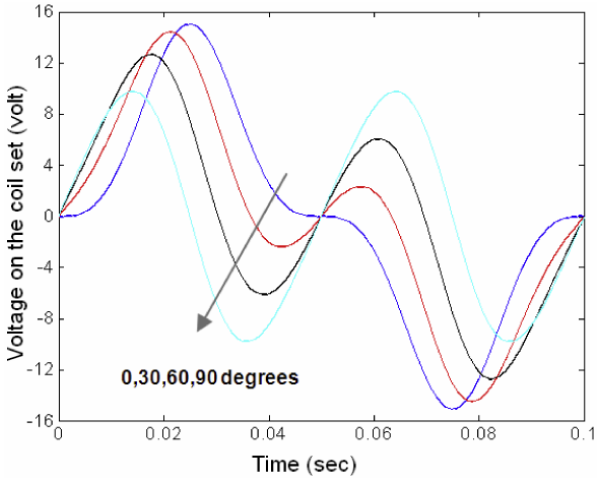

Figure 10. The waveforms (calculated) of regenerated voltage of the coil set at phases 0°, 30°, 60° and 90° under peak-to-peak vibration amplitude $1H$ ($H = 11.35$ mm) and frequency 10 Hz.

Experiment 2: regenerated voltage and excitation frequency. The second experiment was conducted to check the RMS value of the regenerated voltage at different excitation frequencies from 0 to 60 Hz. Coils at the phases 0° and 180° were recorded together, and coils of 90° and 270° phase were also recorded. The shaker excitation voltages are set as 0.25, 0.6, 1, 1.2 and 1.7 V, which correspond to the vibration amplitude (peak-to-peak) around $0.14H$, $0.36H$, $0.61H$, $0.72H$ and $1H$ ($H = 11.35$ mm) at low frequency. Figures 11 and 12 show the experimental results obtained from 0°/180° and 90°/270° phases of the prototype. The frequencies at which peak voltage occurs on the $0/180°$ and $90/270°$ are not the same.

Figures 13 and 14 show the predicted relation of the RMS voltages and frequency of the 0°/180° and 90°/270° phases at DC vibration amplitudes of $0.05H$, $0.25H$, $0.4H$, $0.6H$, $0.75H$ and $1.0H$. The trends closely agree with the experimental results.

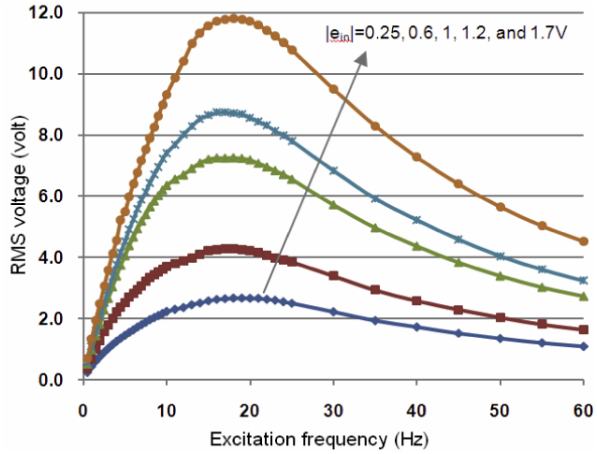

Figure 11. RMS voltage output versus input frequency for 0° phase coil set (eight coils) at different shaker excitation voltages.

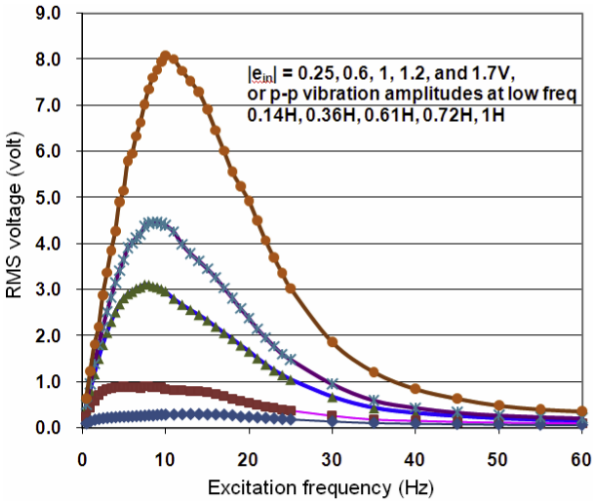

Figure 12. RMS voltage output versus input frequency for 90° phase coil set (eight coils) at different shaker excitation voltages.

Experiment 3: regenerated voltage and excitation amplitude. The third experiment was conducted to analyze the relation between vibration amplitude and the corresponding RMS voltage output. The amplitude of the vibration from the vibration shaker is controlled with the input voltage from the wavefunction generator. At a constant frequency (1, 4 and 10 Hz), input voltage was incrementally increased. RMS output voltages were recorded. The results are shown in figure 15. We see that, at small vibration amplitude, the 0°/180° phases generate more power than 90°/270°; the power increases as the vibration amplitude increases, and power of the four phases will be almost the same when the vibration amplitude is large. The trends are consistent with the theoretical predictions in figures 13 and 14.

Experiment 4: the regenerated voltage and power at different equilibrium positions. The fourth experiment was conducted to check the regenerated power of the four-phase configuration at different equilibrium positions. The 0°/180° and 90°/270°

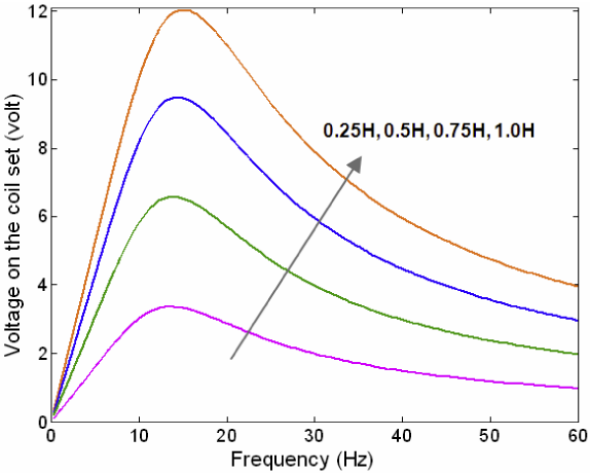

Figure 13. Theoretical prediction: RMS voltages of 0°/180° phase coil at different shaker excitation voltage levels, which correspond to peak-to-peak amplitudes $0.25H$, $0.5H$, $0.75H$, $1.0H$ and $1.0H$ ($H = 11.35$ mm) at low frequency.

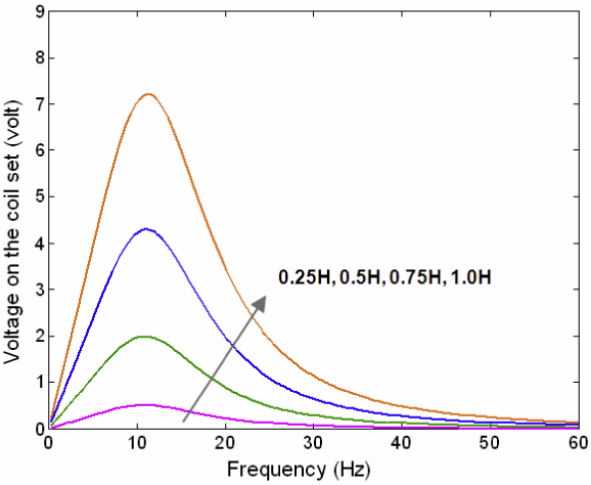

Figure 14. Theoretical prediction: RMS voltage 90° phase coil at different shaker excitation voltage levels, which correspond to peak-to-peak amplitudes $0.25H$, $0.5H$, $0.75H$, $1.0H$ and $1.0H$ ($H = 11.35$ mm) at low frequency.

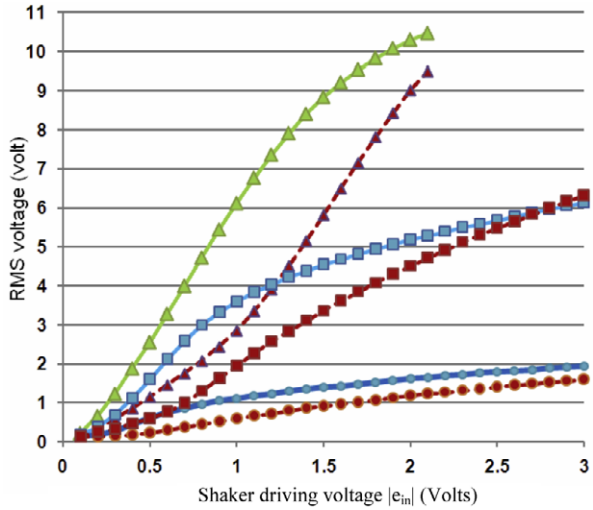

Figure 15. The recorded RMS values of the regenerated voltages versus shaker driving voltage (vibration amplitude) for the eight 0°/180° phase coils (solid) and the eight 90°/270° phase coils (dotted) at different excitation frequencies: 10 Hz (triangle), 4 Hz (square) and 1 Hz (round).

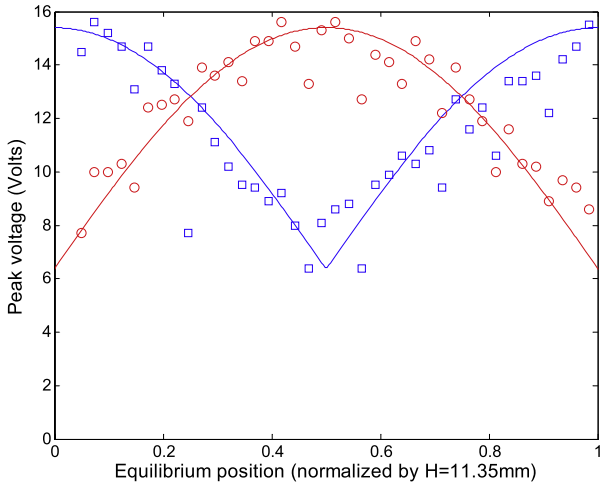

Figure 16. The recorded peak values of the regenerated voltages of 0/180 (square) and 90/270 (circle) degree coils at different equilibrium positions in comparison with theoretical prediction (5 Hz and 1 V excitation).

phase coils were connected for measurement separately. The input to the shaker is set as $e_{\text{in}} = 1$ V. The equilibrium position was adjusted by rotating the $1/4''$-20 threaded rod. Both peak and RMS values of regenerated voltages were recorded. The results of peak values are shown in figure 16 and the RMS values are shown in figure 17. The reason the curves are less smooth than previous experiments is that threaded rod adjustments are not as precise as the frequency or voltage changes. From figure 17 we see that the total regenerated power is independent of the equilibrium positions of the coils in the magnetic field, though the regenerated power of each coil is.

The reason why the total power does not depend on the position can be explained from equation (12), under the assumption that (1) all coils are identical, (2) four-phase configuration (figure 2) and (3) the magnetic field is in sine waveform (figure 7). Equation (12) says one coil at position z_0 generates a voltage

$$V_{z_0} = B_0 L \cos\left\{\frac{\pi z_0}{H} - \frac{\pi v_{\max}}{H\omega}\cos\omega t\right\} v_{\max}\sin\omega t \qquad (14)$$

and its adjacent coil will generate a voltage

$$V_{z_0+90} = B_0 L \sin\left\{\frac{\pi z_0}{H} - \frac{\pi v_{\max}}{H\omega}\cos\omega t\right\} v_{\max}\sin\omega t. \qquad (15)$$

So the combination

$$V_{z_0}^2 + V_{z_0+90}^2 = B_0^2 L^2 v_{\max}^2 \sin^2\omega t \qquad (16)$$

is independent of the equilibrium position z_0. In figures 16 and 17 the solid lines show the fits of peak and RMS voltages

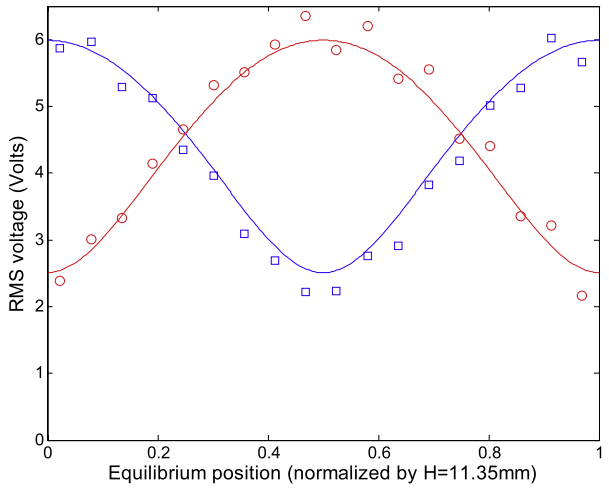

Figure 17. The recorded RMS values of the regenerated voltages of 0/180 (square) and 90/270 (circle) degree coils at different equilibrium positions in comparison with theoretical prediction (10 Hz and 1 V excitation).

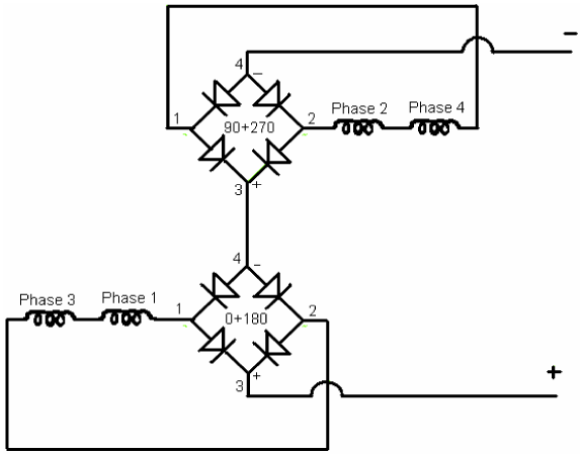

Figure 18. Diagram of AC/DC circuit, where the 0° and 180° phases are connected in series, 0° and 270° phases are connected in series and two rectifiers are used.

according to the analytical predictions of equations (14), and (15).

If all the terminals of the coils are shorted, then the RMS power harvested by the coils can be calculated as

$$P_{\mathrm{RMS}} = \sum \frac{V^2}{R} = \frac{n\sqrt{2}B_0^2L^3v_{\max}^2}{\pi\sigma d^2} \tag{17}$$

where n is the number of coils sets. (In this prototype we have $n = 4$: four sets of 0–90–180–270 phases.)

From the Matlab analysis and waveform observation, the four-phase design was confirmed and the rectifier circuit could be created. It was concluded that the voltage waveform of 0° and 180° phases are out of phase instantaneously and we can simply reverse the heads and tails and connect them together. This also applies to the 90° and 270° phases. But these pairs of 0/180 and 90/270 phases cannot be combined directly. Therefore, the AC/DC circuit was designed, including two rectifiers, as seen in figure 18. Please note that if this circuit is employed the total power harvested will be proportional to $(|V_{z_0}| + |V_{z_0+90}|)^2 = B_0^2L^2v_{\max}^2 \sin^2\omega t\{1 + |\sin(\frac{2\pi z_0}{H} - \frac{2\pi v_{\max}}{H\omega}\cos\omega t)|\}$, which is position-dependent.

Experiment 5: power output of the regenerative shock absorber. The fifth experiment was done to calculate the power of the harvester. The relative vertical velocity, v_z, was determined from Goldner *et al*'s [15] preliminary study of energy recovery. By analyzing smooth road driving conditions of 'typical' highway road profiles and assuming a traveling speed of 20 m s^{-1} (45 mph), it was concluded that the range of vertical relative velocity is 0.2–0.6 m s^{-1}. The experiments were run at 10 Hz and 1.7 V excitation, which corresponds to a 0.25 m s^{-1} vertical velocity (RMS), in the range of the typical relative velocity of suspensions 0.2–0.6 m s^{-1} [15]. The power output of both 0/180 and 90/270 coil sets of the harvester were evaluated (before the rectifier). The RMS voltages are measured as 9.30 V on the 0°/180° coil set (78 Ω) and 8.00 V on the 90°/270° coil set (71 Ω) with outer cylinder. The 1:2 scale prototype is able to regenerate 2.01 W RMS power under 0.25 m s^{-1} RMS relative velocity. Therefore the performance of a full-scale regenerative shock absorber will be estimated as 16–64 W at 0.25–0.5 m s^{-1} RMS suspension velocity. This is the total power we can potentially harvest, and the actual amount of power will further depend on the harvesting power electronics.

The experiment was also conducted without the high magnetically permeable outer cylinder, and the half-scale prototype was only able to generate 8.21 and 5.52 V RMS voltage, corresponding to 1.29 W power at 0.25 m s^{-1} *RMS relative velocity*. Therefore, the high permeable outer cylinder increases the power density by 56%, which agrees well with that in the FEA analysis ($54\% = 1.24^2 - 1$).

4. Conclusions

In this paper we present the design, optimization, analysis and experimental results of a retrofit regenerative shock absorber for vibration energy harvesting from vehicle suspensions. Theoretical predictions and experimental results agree very well. A 1:2 scale prototype of a four-phase linear generator was developed and characterized both experimentally and analytically. The half-scale prototype was able to harvest 2–8 W of energy at 0.25–0.5 m s^{-1} RMS suspension velocity. It was also found that the frequency of the regenerated voltage does not necessarily have the same frequency as the excitation. Instead, the wave shapes of the regenerated voltage will depend on excitation frequency, amplitude and equilibrium position. The regenerated power will be the largest at a frequency around the resonance of the vibration system. Though the voltage waveform of the individual coil depends on the equilibrium position, the total power of the four phases does not depend on it.

Further research is underway to improve the energy density and efficiency by taking the harvesting electrical circuit and the harvester output resistance into account.

References

[1] Melosi M V 2004 The automobile and the environment in American history *Automobile in American Life and Society* (Dearborn: University of Michigan Press)

[2] *The Columbia Electronic Encyclopedia* 2007 6th edn (New York: Columbia University Press)

[3] Energy Information Administration *Basic Petroleum Statistics* http://www.eia.doe.gov/basics/

[4] *Economic Report of the President* http://www.whitehouse.gov/cea/ch6-erp07.pdf

[5] *Advanced Technologies and Energy Efficiency* http://www.fueleconomy.gov/FEG/atv.shtml

[6] Suda Y and Shiba T 1996 New hybrid suspension system with active control and energy regeneration *Veh. Syst. Dyn.* **25** (Suppl.) 641–54

[7] Suda Y, Nakadai S and Nakano K 1998 Hybrid suspension system with skyhook control and energy regeneration (Development of self-powered active suspension) *Veh. Syst. Dyn.* **19** (Suppl.) 619–34

[8] Nakano K and Suda Y 2004 Combined type self-powered active vibration control of truck cabins *Veh. Syst. Dyn.* **41** 449–73

[9] Nakano K, Suda Y and Nakadai S 2003 Self-powered active vibration control using a single electric actuator *J. Sound Vib.* **260** 213–35

[10] Jolly M R and Margolis D L 1997 Assessing the potential for energy regeneration in dynamic subsystems *J. Dyn. Syst. Meas. Control* **119** 265–30

[11] Jolly M R and Margolis D L 1997 Regenerative systems for vibration control *J. Vib. Acoust.* **119** 208–15

[12] Okada Y, Harada H and Suzuki K 1997 Active and regenerative control of an electrodynamic-type suspension *JSME Int. J. Ser.* C **40** 272–8

[13] Kim S S and Okada Y 2002 Variable resistance type energy regenerative damper using pulse width modulated step-up chopper *J. Vib. Acoust.* **124** 110–5

[14] Graves K E, Iovenitti P G and Toncich D 2000 Electromagnetic regenerative damping in vehicle suspension systems *Int. J. Veh. Des.* **24** 182–97

[15] Goldner R B, Zerigian P and Hull J R 2001 A preliminary study of energy recovery in vehicles by using regenerative magnetic shock absorbers *SAE Paper #2001-01-2071*

[16] Bose suspension system-white paper, Bose Company 2004 http://www.bose.com/

[17] Paz O D 2004 Design and performance of electric shock absorber *Master's Thesis* Louisiana State University

[18] Goldner R B and Zerigian P 2005 Electromagnetic linear generator and shock absorber *US Patent Specification* 6,952,060 B2 (inventors; Trustees of Tufts College, assignee. Oct. 4 2005)

[19] Gupta A, Jendrzejczyk J A, Mulcahy T M and Hull J R 2006 Design of electromagnetic shock absorbers *Int. J. Mech. Mater. Des.* **3** 285–91

[20] Song X and Li Z 2005 Regenerative damping method and apparatus *US Patent Specification* 6920951

[21] Song X, Li Z and Edmonson J R 2006 Regenerative passive and semi-active suspension *US Patent Specification* 7087342

[22] Amati N, Canova A, Cavalli F, Carabelli S, Caviasso G, Festini A and Tonoli A 2006 Electromagnetic shock absorbers for automotive suspensions: electromechanical design *8th Biennial ASME Conf. on Engineering Systems Design and Analysis (Torino 2006)*

[23] Zhang Y, Huang K, Yu F, Gu Y and Li D 2007 Experimental verification of energy-regenerative feasibility for an automotive electrical suspension system *2007 IEEE Int. Conf. on Vehicular Electronics and Safety*

[24] Kubota T and Inoue H 2008 Electromagnetic suspension devices *European Patent Application* #EP1985476A1

[25] Kawamoto Y, Suda Y, Inoue H and Kondo T 2008 Electro-mechanical suspension system considering energy consumption and vehicle manoeuvre *Veh. Syst. Dyn.* **46** 1053–63

[26] *Finite Element Method Magnetics* http://femm.foster-miller.net/wiki/